[99mTc]-labelled interleukin-8 as a diagnostic tool compared to [18F]FDG and CT in an experimental porcine osteomyelitis model

Afzelius, Pia; Heegaard, Peter Mikael Helweg; Jensen, Svend Borup; Alstrup, Aage Kristian Olsen; Schønheyder, Henrik Carl; Eek, Annemarie; Boerman, Otto; Nielsen, Ole Lerberg

Published in:
American Journal of Nuclear Medicine and Molecular Imaging

Publication date:
2020

Document Version
Publisher's PDF, also known as Version of record

Am J Nucl Med Mol Imaging 2020;10(1):32-46
www.ajnmmi.us /ISSN:2160-8407/ajnmmi0106253

Original Article

[^{99m}Tc]-labelled interleukin-8 as a diagnostic tool compared to [^{18}F]FDG and CT in an experimental porcine osteomyelitis model

Pia Afzelius[1,6], Peter Mikael Helweg Heegaard[7], Svend Borup Jensen[1,2], Aage Kristian Olsen Alstrup[3], Henrik Carl Schønheyder[4,5], Annemarie Eek[8], Otto Boerman[8], Ole Lerberg Nielsen[9]

[1]Department of Nuclear Medicine, Aalborg University Hospital, Aalborg, Denmark; [2]Department of Chemistry and Biochemistry, Aalborg University, Aalborg, Denmark; [3]Department of Nuclear Medicine and PET, Aarhus University Hospital, Skejby, Denmark; [4]Department of Clinical Microbiology, Aalborg University Hospital, Aalborg; [5]Department of Clinical Medicine, Aalborg University, Aalborg; [6]North Zealand Hospital, Hillerød, University Hospital of Copenhagen, Denmark; [7]Department of Biotechnology and Biomedicine, Danish Technical University, DTU, Lyngby, Denmark; [8]Department of Radiology and Nuclear Medicine, Raboud UMC, Nijmegen, The Netherlands; [9]Department of Veterinary and Animal Sciences, Faculty of Health and Medical Sciences, University of Copenhagen, Copenhagen, Denmark

Received October 29, 2019; Accepted February 7, 2020; Epub February 25, 2020; Published February 28, 2020

Abstract: Osteomyelitis (OM) is an important cause of morbidity and sometimes mortality in children and adults. Long-term complications can be reduced when treatment is initiated in an early phase. The diagnostic gold standard is microbial examination of a biopsy and current non-invasive imaging methods are not always optimal. [^{111}In]-leukocyte scintigraphy is recommended for peripheral OM, but is time-consuming and not recommended in children. [^{18}F]FDG PET/CT is recommended for vertebral OM in adults, but has the disadvantage of false positive findings and a relatively high radiation exposure; the latter is a problem in children. [^{99m}Tc]-based tracers are consequently preferred in children. We, therefore, aimed to find a [^{99m}Tc]-marked tracer with high specificity and sensitivity for early detection of OM. Suppurating inflammatory lesions like OM caused by *Staphylococcus aureus* (*S. aureus*) will attract large numbers of neutrophils and macrophages. A preliminary study has shown that [^{99m}Tc]-labelled IL8 may be a possible candidate for imaging of peripheral OM. We investigated [^{99m}Tc]IL8 scintigraphy in a juvenile pig model of peripheral OM and compared it with [^{18}F]FDG PET/CT. The pigs were experimentally inoculated with *S. aureus* to induce OM and scanned one week later. We also examined leukocyte count, serum CRP and IL8, as well as performed histopathological and microbiological investigations. [^{99m}Tc]IL8 was easily and relatively quickly prepared and was shown to be suitable for visualization of OM lesions in peripheral bones detecting 70% compared to a 100% sensitivity of [^{18}F]FDG PET/CT. [^{99m}Tc]IL8 is a promising candidate for detection of OM in peripheral bones in children.

Keywords: Animal model, pig, swine, porcine, [^{99m}Tc]IL8, scintigraphy, [^{18}F]FDG, PET, CT, SPECT/CT, osteomyelitis, *staphylococcus aureus*

Introduction

Osteomyelitis (OM) is a severe disease in childhood, especially in the low income part of the world [1, 2]. Acute OM often occurs in children and is frequently located in the long bones. In high-income countries, the annual incidence is 13 per 100,000 (acute OM is 8 and sub-acute OM 5 per 100,000). The incidence is higher in children under the age of 3 years than in older children [3]. Severe complications include sequester and fistulous tract formation, which may ultimately lead to severe deformity of the affected bone and reduce the quality of life [1, 2]. It is therefore pivotal to diagnose the infection in an early state, when curable with antibiotic treatment and thus avoid disabling sequelae.

There are different routes of the establishment of OM of which the hematogenously spread of a microorganism is the most frequent. In 95 percent of the cases, the microorganism is *Staphylococcus aureus* (S. *aureus*) [4]. We have therefore developed a juvenile pig OM model for hematogenously spread *S. aureus* [5, 6].

The gold standard for the diagnosis of osteomyelitis is bone biopsy with histopathological and

tissue culture examination. This will ideally direct adequate treatment against the specimen obtained. However, this is an invasive procedure and noninvasive imaging is often preferred and used for initiation of empirical antimicrobial treatment.

Plain radiographs are often the first step in the assessment of OM, since they are inexpensive, available, and safe, however radiographic images show changes only in advanced stages of OM, when at least 50 to 75% of the bone is destructed, which is typically first detectable more than 2 weeks after the infection has started [7].

Computed tomography (CT) and magnetic resonance imaging (MRI) can also be used for diagnosis and evaluation of OM. Both modalities show excellent anatomic detail, including the destruction of bone cortex, sequester and fistula formation, and soft tissue involvement. CT can visualize trabecular bone loss if more than 50-75% of the bone is lost, but has higher spatial resolution than plain radiography and MRI. In addition, it is a useful technique for imaging-guided needle biopsy and for aspirating material for microbiological examination [8]. Also, CT is more widely available and image-acquisition is faster than for MRI. However, CT contributes to ionizing radiation exposure and application in children is only advisable after careful consideration. Magnetic Resonance Imaging is the modality of choice for early detection of acute OM. Bone marrow changes can be detected within three to five days after disease onset by Fat-Sat T2-weighted imaging [9]. Magnetic Resonance Imaging is, however, expensive, image-acquisition takes longer time, anesthesia may be necessary, and it is not always available. In general, nuclear medicine techniques have a high sensitivity for detection of osteomyelitis by allowing imaging of the whole skeleton to look for multiple sites of infection but are limited by both poor specificity and poor anatomical localization [10]. Hybrid imaging techniques such as single photon emission computed tomography/CT (SPECT/CT) and positron emission computed tomography/CT (PET/CT) provide more precise anatomical information than the conventional nuclear medicine techniques.

Bone scintigraphy with [^{99m}Tc] methylene diphosphonate is more sensitive in detecting the early stages of bone repair than radiography and lesions in the whole skeleton is easily diagnosed by this method [8]. The specificity has been reported to be low, as the tracer accumulates in any area with increased bone turnover [11-13]. This, however, also depends on the stage of the disease and on the age of the patient [14]. Previously we have seen that [^{99m}Tc] methylene diphosphonate did not accumulate in OM of juvenile pigs inoculated with *S. aureus* [15], probably due to a more advanced stage according to the Cierny-Mader staging [16-18] of OM than would be expected after just one week of infection.

Leukocyte scintigraphy is the gold standard in nuclear medicine for visualizing OM in the peripheral bones [19]. This imaging procedure has a higher specificity for OM than bone scan (>90% versus 80%) and a sensitivity of 78% [20], however the sensitivity decreases from 84 to 21% for chronic osteomyelitis in the axial skeleton, which is "poorly understood, but micro thrombotic occlusion and inflammatory compression of the blood vessels may prevent labelled cells from reaching the site of infection" [21]. The preparation of radiolabeled autologous white blood cells is time-consuming and there is radiation exposure to the personnel and a minor risk of cross-contamination between patients [19]. [^{18}F]FDG PET/CT is recommended for vertebral OM in adults, but neither PET-tracers nor ^{111}In-based tracers are recommended for an examination of children. We, therefore, searched for other tracers with higher specificity and sensitivity in a porcine juvenile subacute OM model, and we have demonstrated a high sensitivity for [^{18}F]FDG obviating leukocyte scintigraphy in juvenile pigs [15].

Suppurating inflammatory lesions like OM caused by *S. aureus* will attract large numbers of neutrophils and macrophages [22, 23]. Neutrophils express two types of interleukin-8 (IL8) receptors i.e.; the G-protein coupled C-X-C motif chemoreceptors 1 and 2 (CXCR1 and CXCR2) [22]. IL8 (also denoted CXCL8) acts in humans as a chemo-attractant, and a primer and activator of neutrophils during inflammation in various contexts [22-28]. Neutrophils, like several other cell types, have the capacity of IL8 synthesis following a pro-inflammatory stimulus [29]. IL8 is secreted by isolated lipopolysaccharide-stimulated porcine pulmonary alveolar macrophages and has chemotactic activity towards neutrophils [30], and upregulation of IL8 receptors in various organs has been verified during inflammatory and infectious diseases in

the pig [31, 32]. IL8 is produced by osteoclasts [33] and stimulates osteoclast genesis and bone resorption independent of the RANKL pathway [34] and may be important for the RANKL-induced osteoclast formation [35]. In a previous study, Gross et al. showed that [^{131}I]-labelled IL8 could visualize OM lesions in active foot infections of diabetic patients [36]. However, Rennen et al. have demonstrated that radiolabeling with iodine clearly affected the *in vivo* bio-distribution of IL8 [37] and that labelling with [^{99m}Tc] was preferable compared to [^{131}I] for clinical applications as the targets to background was superior and the radiation exposure was lower [37]. Therefore, [^{99m}Tc]-labelled IL8 has been selected and tested as a possible alternative to leukocyte scintigraphy for imaging of acute OM.

In this study, we compared [^{99m}Tc]-labelled IL8 with [^{18}F]FDG as a tracer to diagnose experimental *S. aureus* OM in peripheral bones in a set of ten juvenile pigs inoculated with *S. aureus* one week before scanning.

Materials and methods

S. aureus-induced OM model in juvenile pigs

Ten pigs (numbered consecutively), all clinically healthy, specific pathogen-free Danish Landrace Yorkshire cross-bred female pigs aged 8-9 weeks having a weight of 19.0-24.5 kg, were purchased from local commercial pig farmers. After one week of acclimatization, the pigs were fasted over-night, premedicated with s-ketamine (Pfizer, Ballerup, Denmark) and midazolam (B. Braun Medical, Frederiksberg, Denmark) intramuscularly, anesthetized with propofol (B. Braun Medical, Frederiksberg, Denmark) intravenously, and inoculated with a well-characterized porcine strain of *S. aureus* (10,000 CFU/kg body weight) into the femoral artery of the right hind limb to induce OM in that limb, as described elsewhere [5]. After onset of clinical signs, e.g. limping of the right hind limb, redness, and local swelling of the leg, starting typically day 3-4 after inoculation, the pigs were supplied with intramuscular procaine benzylpenicillin (10,000 IE)/kg procaine benzylpenicillin (Penovet, Boehringer Ingelheim, Copenhagen, Denmark) once daily until 48 hours before scanning [6]. The pigs were treated with 30-45 μg/kg buprenorphine (Indivier, Birkshire, United Kingdom) IM thrice daily from inoculation and until scanning at day 6 and 7 after inoculation [6]. After scanning, pigs were euthanized with an overdose of pentobarbitone (Scan Vet Animal Health, Fredensborg, Denmark) while still under anesthesia.

Humane endpoints were: anorexia for more than 24 hours, superficial respiration, or the inability to stand up. After the inoculation, pigs were housed in separate boxes, fed twice daily with restricted standard pellet diet (DIA plus FI, DLG, Denmark) and had *ad libitum* access to tap water. The environment was characterized by a room temperature of 20°C, a relative humidity of 51-55%, 12 hours light cycles, an exchange of air eight times per hour. Pigs were fasted overnight prior to anesthesia.

The study was approved by the Danish Animal Experimentation Board, license no. 2012-15-2934-000123 and 2017-15-0201-01239. All facilities were approved by the Danish Occupational Health Surveillance.

White blood cells counts, serum C-reactive protein and serum IL8

Blood samples were drawn on day 0 (inoculation), day 6 (diagnostic CT scan) and day 7 (scintigraphy, SPECT and PET/CT). White blood cell counts, including a leukocyte differential count were performed by the Veterinary Diagnostic Laboratory, Department of Veterinary Clinical Sciences, University of Copenhagen, Copenhagen using EDTA-stabilized whole blood and an automated complete blood cell counter (ADVIA 120 analyzer, Bayer Healthcare Diagnostics, Berlin, Germany).

Serum C-reactive protein (CRP) measurements were performed according to Heegaard et al. [38]. Briefly, a sandwich Enzyme-Linked ImmunoSorbent Assay (ELISA) using dendrimer-coupled cytidine diphosphocholine in the coating layer was used employing polyclonal rabbit anti-human antibodies with cross-reactivity towards porcine CRP followed by a peroxidase-conjugated goat-anti-rabbit antibody for detection (both antibodies from DAKO, Glostrup, Denmark). Plates were developed with a tetramethylbenzidine (TMB) peroxide color substrate (Kem-En-Tec, Taastrup, Denmark). Pooled pig serum calibrated against a human CRP calibrator (DAKO A0073) was used as standard. All samples were run in duplicates. The detection limit was 1.42 mg/L (human equivalents).

Porcine IL8 was measured in serum in a Duoset ELISA from R&D Systems (Duoset DY535, R&D Systems, Abingdon, UK) which is a sandwich ELISA using mouse anti-pig IL8 for catching and biotinylated goat anti-IL8 for detection, also including a porcine IL8 standard. According to the manufacturer, this ELISA shows negligible cross-reaction with human IL8. After incubation with peroxidase-streptavidin also supplied in the kits, plates were developed as described above. All samples were run in duplicates in a dilution of 1:2 with a detection limit of 62.5 pg/mL.

Microbiology

The inoculum was prepared from the S54F9 strain of *S. aureus*, isolated from a chronic embolic pulmonary abscess in a pig [39]. The strain is pan-susceptible for antibiotics and the signs of OM were modifiable with procaine penicillin. Swaps and tissue biopsies were obtained *post mortem* for bacteriological culture to confirm the bacterial agent.

Conjugation of HYNIC to IL8

Recombinant human IL8 (ProSpec catalogue no. chm-231, lot number 906PIL821, Ness Ziona, Israel) was stored at -20°C. *N*-(Tris (hydroxymethyl)-methyl) glycine (Tricine) was purchased from Sigma-Aldrich (Zwijndrecht, The Netherlands), glycine was obtained from Sigma-Aldrich. Polyoxyethylenesorbitan monooleate (Tween 80) was bought from Genfarma (Toledo, Spain). 2-(*N*-morpholino) ethanesulfonic acid (MES) were purchased from Sigma-Aldrich and 6-hydrazinonicotinic acid (HYNIC) was obtained from Solulink (San Diego, USA).

The IL8-HYNIC conjugate was prepared as described previously [40], with minor modifications. In brief, 500 µg of synthetic human IL8 was reconstituted in 45 µL of water and incubated for 30 minutes at 4°C. After that 45 µl of buffer (0.1 M MES, pH 6.5 and 0.64 M Sodium chloride (NaCl) (Merck, Darmstadt, Germany) and 10 µL of 1.0 M Sodium hydrogen carbonate ($NaHCO_3$) Merck (Darmstadt, Germany), pH 8.2 were added. Subsequently, a 3-fold molar excess of HYNIC in 10 µL of dry dimethyl sulfoxide (Sigma-Aldrich, Zwijndrecht, The Netherlands) was added dropwise to the mixture. After incubation for 10 min at room temperature, the reaction was stopped by the addition of an excess of glycine (100 µL); 1.0 M glycine in phosphate-buffered saline (PBS) (B. Braun) (Oss, The Netherlands). Next, 0.8 mL of 0.05% Tween 80 in PBS was added, and the mixture was purified on a PD10 column (GE Healthcare, Woerden, the Netherlands) to remove excess unbound HYNIC.

Radiolabelling procedure

Two vials of IL8-HYNIC (10 µg) and a vial containing 1.0 mL of the reduction solution (a mixture of 50 µg Tin sulphate ($SnSO_4$) (Sigma-Aldrich, Zwijndrecht, The Netherlands), 75 mg Tricine and 7.5 mg nicotinic acid (Sigma-Aldrich, Zwijndrecht, The Netherlands) in PBS) were thawed. To prepare the reduction solution, the $SnSO_4$, Tricine and nicotinic acid (C_6H5NO_2) were dissolved in 0.1 M Hydrochloric acid (HCl) (Merck, Darmstadt, Germany), while continuously bubbling the solution with nitrogen gas. The pH was then adjusted to 5.5-6.0 with 1.7 M Natrium hydroxide (NaOH) (Merck, Darmstadt, Germany) and the final volume was adjusted with water (H_2O) (Versol, (Lyon, France). Aliquots of this mixture were stored under nitrogen gas at -20°C.

One of the 10 µg IL8-HYNIC vials was used as the reactor for the radiolabeling reaction, the content of the other 10 µg IL8-HYNIC vial was transfer into the reactor by adding 800 µL of the reducing solution to it and then transferred the mixture to the reaction vial so that the combined contents of the reactor was 20 µg IL8-HYNIC and 40 µg $SnSO_4$, 60 mg Tricine and 6.0 mg nicotinic acid.

Then 1250-1900 MBq of [^{99m}Tc]pertechnetate was added. The mixture was incubated at 70°C for 20 min. The radiochemical purity was determined by instant thin-layer chromatography on ITLC-SG strips (Biodex, Shirley, NY, USA) with 0.1 M citrate, pH 6.0 as the mobile phase (R_f of the [^{99m}Tc] IL-8-HYNIC is 0.0-0.2, the R_f of non-incorporated [^{99m}Tc] pertechnetate is 0.8-1.0). The efficiency of the labelling reaction was higher than 98%. After the labelling reaction was complete, the reaction mixture was diluted with a 0.9% Sodium chloride (NaCl) (Merck, Darmstadt, Germany) solution to a final concentration of 100-125 MBq/mL. Syringes ready for injection were prepared. The radioactivity of the syringes was measured prior to and after injection. Pigs received ~400 MBq (range: 310-

Table 1. Tracers and scans

Pig	[^{99m}Tc]IL8 MBq injected at time 0	Whole Body Scintigraphy min after injection of tracer	SPECT/CT min after injection of tracer	[^{18}F]FDG MBq injected at time 0	PET min after injection of tracer
1	370	139	165	149	60
2	***310***	***256***	***294***	***103***	***67***
3	420	140	164	94	66
4	380	341	366	100	115
5	350	239	265	111	60
6	390	150	175	100	60
7	440	258	283	103	79
8	***433***	***122***	***150***	***95***	***79***
9	434	235	265	120	64
10	550	145	170	119	61

Tracer and scanning characteristics. Pig 2 and 8 are marked by bold italic as these pigs did not develop OM.

550 MBq) corresponding to 13.1-23.2 MBq/kg [^{99m}Tc]IL8 per animal and to ~ 6.7 μg IL8 intravenously 165-366 minutes prior to performing the scintigraphy (**Table 1**) [40].

[^{18}F]FDG

[^{18}F]FDG was produced by a standard procedure applying a GE Healthcare MX Tracerlab synthesizer, Mx cassettes supplied by Rotem Industries (Arava, Israel) and chemical kits supplied by ABX GmbH (Radeberg, Germany). Radiochemical purity was higher than 99%. Normal recommended injected activity for children is 3.7-5.2 MBq per kg. The average injected activity (**Table 1**) was as 110 MBq (range 94-149 MBq), corresponding to 4-6.3 MBq/kg. The PET was performed ~ 66 min (60-79 min, **Table 1**) after injection of [^{18}F]FDG.

CT, scintigraphy, SPECT, and PET

Diagnostic CT scans were performed one day prior to the other scans, i.e. day 6 to evaluate if lytic lesions had developed.

The pigs were placed in dorsal recumbence during Propofol anesthesia while they were mechanically ventilated and CT scanned applying an integrated system (GE VCT discovery True 64 PET/CT 2006, GE Healthcare, USA) Reflexes, pulse, oxygen saturation, and body temperature were monitored. Initially, a scout view was obtained to secure body coverage from snout to tail.

Anesthetized, ventilated, monitored pigs were again placed in dorsal recumbent position on day 7 and PET/CT scanned applying an integrated system (GE VCT discovery True 64 PET/CT 2006, GE Healthcare, USA), with one bed position spanning 15 cm. PET images were reconstructed using an iterative algorithm (ViewPoint algorithm, GE Healthcare) and attenuation correction based on low-dose CT.

Planar gamma imaging and Single Photon Emission Computed Tomography (SPECT)/CT were performed using a Symbia T16 SPECT/CT (Siemens Medical Solutions, Hoffman Estates, Illinois, USA). The residual activity from PET isotopes was detected as background radiation on the SPECT scanner. To minimize the interference of this 511 keV background activity, we applied the medium-energy collimator [41]. Whole-body, planar images were acquired using dual-headed simultaneous anterior and posterior whole-body acquisition.

Reading the scans

Positron emission tomography with [^{18}F]FDG, SPECT with [^{99m}Tc]IL8, and CT scans were read individually. PET and scintigraphy were also read as fused images with CT. All scans were evaluated by an experienced nuclear medicine specialist with CT competences. OM lesions were identified on CT and the OM volumes were calculated as an approximation measured in three planes.

Necropsy, histopathology, and immunohistochemistry (IHC)

The pigs were necropsied as described [42]. During necropsy, swabs and biopsies were

Table 2. Pig characteristics

Pig	Body weight/ kg	Neutrophil counts day 0 10^9/L	Neutrophil counts day 7 10^9/L
1	23.6	n.t	5.2
2	***23.6***	***7.1***	***15.2***
3	23.6	n.t.	7.1
4	19.3	6.2	n.t.
5	20.1	4.9	10.1
6	19.0	6.0	9.9
7	19.0	6.1	8.6
8	***20.0***	***4.2***	***9.9***
9	20.5	4.1	13.6
10	24.5	5.0	10.3

Pig 2 and 8 are marked by bold italic as these pigs did not develop OM. n.t: not tested as the blood sample was missing.

sampled for microbial cultivation, and selected tissues and organs were sampled for histopathology: right phalangeal bones from pig 9 and 10, lung tissue from pig 2 and 8, and kidney from pig 8. Tissues and organs were fixed in 3.7% neutral buffered formaldehyde for 4 days to 12 months and bones were decalcified for 3 weeks using 3.3% formaldehyde with 17% formic acid. Hematoxylin and eosin (HE) staining was carried out using standard procedures. The IHC identification of *S. aureus* and IL8 was performed as presented [43, 44]. We acquired sufficient CT, macroscopic, bacteriological, and histopathological findings to confirm or reject the diagnoses. Specifically, the pigs were defined as having attained infection with the inoculated *S. aureus* if bacterial culture and/or *S. aureus* IHC confirmed the presence of *S. aureus* in one or several lesions in each individual pig.

Statistics

IBM SPSS version 22 was used for the statistical analyses.

Pearson r correlation was used for correlations. According to the classification system by Salkin, *r* values between 0.8 and 1.0 represent a very strong correlation, between 0.6 and 0.8 a strong correlation, between 0.4 and 0.6 a moderate correlation, and between 0.2 and 0.4 a weak correlation. Values between 0.0 and 0.2 are classified as showing a weak or no correlation [45]. A t-test was used for comparing groups. A paired t-test was used comparing infected and not infected limbs. A significance level of <0.05 was considered significant.

Results

[^{99m}Tc]-labelling of IL8

The radiochemical purity of the [^{99m}Tc]IL8 preparation was higher than 98%, determined by instant thin-layer chromatography, excluding the need for further purification. The specific activity of the [^{99m}Tc]IL8 preparations used in this study was approximately 60 MBq/μg IL8.

Infection model

As the tubular bones, such as tibia and femur, are the most common sites of infection in children, we used the juvenile OM pig model as it develop OM in the exact same location as in children [5, 15, 46]. After *S. aureus* inoculation of the juvenile pigs (19-24.5 kg, **Table 2**) there was a significant increase of mean neutrophil counts at day 0 and 7 from 5.4 to 10.0 × 10^9/mL, respectively (**Table 2**). Mean CRP increased ~ 60-fold from day 0 to day 6 with a slight decrease day from day 6 to day 7 in the eight pigs that developed OM (**Figure 1**). The difference between day 0 and day 6 was statistically significant (P=0.014) for pigs with OM as well as between day 0 and day 7 (P=0.006). There was no statistical significance between day 6 and 7 (P=0.322) for the pigs with OM.

In the two pigs that did not develop OM, the mean CRP increased ~ 6-fold day six and 18-fold day seven (**Figure 1**). None of the pigs reached the humane endpoint as specified in the protocol of the study.

Some data from these pigs have been presented previously in earlier studies (see legends in **Table 3**). Histopathology and IL8 IHC of the right proximal phalanx from toe IV of pig 9 revealed presence of a subacute abscess with sequestrated bone and fistulation in the metaphysis, and presence of cells, mainly neutrophils, that were IL8 positive (**Figure 2**). Thus, both pathologically and according to the Cierny-Mader classification, the infection appeared to be subacute or even chronic as early as 7 days after the inoculation of *S. aureus*. *S. aureus* was re-isolated from OM lesions or periosseous abscesses in pigs 1 and 3-7, and from the

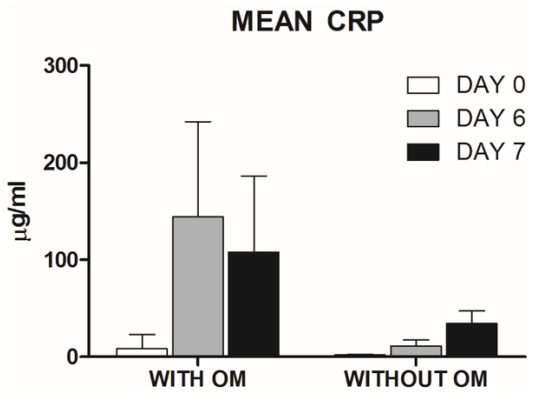

Figure 1. Mean serum concentration of CRP in µg/ml and error bars in pigs with OM (n=8) and without OM (n=2) measured before (white boxes), 6 days after (gray boxes) and 7 days after (black boxes) inoculation with *S. aureus*. The diference between day 0 and day 6 was statistically (P=0.014) significant for pigs with OM as well as between day 0 and day 7 (P=0.006). There was no statistical significans between day 6 and 7 (P=0.322) for the pigs with OM.

inoculation site abscess in pig 9 (OM or periosseous lesions not tested). *S. aureus* was identified by IHC and microbiological examination in an OM lesion in pig 10. Pigs 2 and 8 did not develop OM, however, an inoculation site abscess was identified by CT and also by FDG (**Table 3**).

Imaging

CT-scans: CT scans revealed the presence of OM lesions in eight of the ten pigs (**Table 3**); two pigs, pig 2 and 8, did not develop any OM lesions.

A total of 23 OM lesion sites developed in the pigs after inoculation. They were all identified by [^{18}F]FDG PET and CT. 16 of the 23 OM (~70%) were identified by [^{99m}Tc]IL8 (**Table 3**). There was no pattern of degree of [^{99m}Tc]IL8-uptake concerning the anatomical location. 21 OM lesion sites had developed sequesters and 19 had developed fistulous tracts.

Scintigraphy of osteomyelitis

The data for the radioactive tracers are listed in **Table 1**. Time from the injection of the tracer to scintigraphy varied from ~ 2 to 6 h. [^{99m}Tc]IL8 uptake did not depend on the time from injection to scan in OM (P=0.69), but in the non-infected contra-lateral anatomical sites, there was a negative strong correlation between time from injection to scan (r=-0.64, P=0.001), indicating a transient uptake in non-infected bones. [^{99m}Tc]IL8 uptake in OM lesions correlated moderately and positively with the injected activity of [^{99m}Tc]IL8 (r=0.5, P=0.016). [^{18}F]FDG uptake in OM lesions correlated positively with the injected [^{18}F]FDG activity (P=0.030).

[^{99m}Tc]IL8 also accumulated variably in non-infected (**Table 4**) and in various infected areas in other locations in the body, such as in 2 out of 7 soft tissue abscesses of the neck (identified by CT [46]) and at the site of inoculation, and in pulmonary infections (**Table 3**).

Single photon emission computed tomography (SPECT) (**Figure 3**) shows the bio-distribution of [^{99m}Tc]IL8 in a pig without OM (pig 8). For comparison, a maximum intensity projection (MIP) of [^{18}F]FDG is included for the same pig. The uptake of IL8 in various organs (cpm) and the maximal Standardized Uptake Value (SUV_{max}) for [^{18}F]FDG are shown in **Table 4** in the non infected pigs. The main difference is the marked uptake of [^{99m}Tc]IL8 in the parenchyma of the kidneys and the relatively low excretion through the urinary tract during the scan period which was not observed with [^{18}F]FDG. Another major difference is the high uptake of [^{18}F]FDG in the heart.

As shown in **Figure 3**, [^{99m}Tc]IL8 accumulated in the epiphysis and growth zones of long bones, in vertebrae, lungs, liver, spleen, and kidneys. The tracer was excreted/metabolized by the kidneys. **Figure 4** shows accumulation in another pig that was without OM (pig 2) of [^{99m}Tc]IL8 in the caudal parts of the lungs and also in the areas of atelectasis (right lung) that developed during the experiment.

In **Figure 5**, the accumulation of [^{18}F]FDG and [^{99m}Tc]IL8 is shown in 3 OM lesions located in the proximal fibular, the proximal tibial, and the III metatarsal bone of pig 4. Diagnostic CT scans the day before showed both sequester and fistulous tract formation of all three OM lesions (**Figure 5**). In **Table 5** the uptake of tracers is listed in OM lesions. [^{99m}Tc]IL8 was physiologically accumulating at the ends of the long bones (**Figures 3** and **5**), but [^{99m}Tc]IL8 accumulation was higher (P<0.00001) and more focal (**Figure 5**) in the infected bone lesions than in the contra-lateral corresponding anatomical sites in the non-infected bones. There was no correlation between [^{99m}Tc]IL8 uptake in the right infected limb and in the left limb without OM (r=0.08, P=0.74).

Table 3. Lesions by CT, necropsy, microbiology, and scans

Pigs Lesions and findings		1	***2***	3	4	5	6	7	***8***	9	10
Osteomyelitis (OM)	CT[1]	5	***0***	3	3	5	1	2	***0***	3	1
	Necropsy	4	***0***	3	3	3	1	2	***0***	2[2]	0[3]
	Microbiology[4]	+	***n.t.***[5]	+	+	+	+	+	***n.t.***	n.t.	+[6]
	[^{18}F]FDG[1]	5	***0***	3	3	5	1	2	***0***	3	1
	[^{99m}Tc]IL8[1]	2	***0***	0	3	4	1	2	***0***	3	1
Inoculation site abscess	CT[7]	-	**+**	-	+	+	+	+	**-**	+	(+)
	Necropsy	-	**-**[7]	-	+	+	+	+	**-**	+	+
	Mircobiology[4]	n.t.	**-**	n.t.	+	+	+	+	***n.t.***	+	+[8]
	[^{18}F]FDG	-	***(+)***	-	-	(+)	+	+	**-**	+	(+)
	[^{99m}Tc]IL8	-	**-**	-	-	(+)	+	+	**-**	(+)	-
Lungs with pneumonia	CT	-	**-**	+	-	-	-	+	**-**	-	+
	Necropsy	-[9]	**-**[9]	+[10]	-	-[11]	-[9]	+	**-**[11]	-[11]	+
	Microbiology	-	**-**	-	-	-	-	+	**-**	-	+[12]
	[^{18}F]FDG	(+)	**-**	-	-	-	(+)	+	**-**	+	+
	[^{99m}Tc]IL8	(+)	**+**	(+)	-	-	(+)	+	***(+)***	-	-

[^{99m}Tc]IL8 and [^{18}F]FDG accumulation in OM and abscesses in the right inguinal region and in neck muscles (Temgesic injections). Pig 2 and 8 are marked by bold italic as these pigs did not develop OM. Some data from the pigs have been published previously: pigs 1, 3, 4, 6, 7, 9, 10 [53]. +; identified. (+); identified, but more difficult to detect. 1: Number of OM lesions sites; thus by Computed Tomography (CT), [^{18}F]FDG and [^{99m}Tc]IL-8 OM lesions were defined by location, not the number, i.e. presence in distal femur, proximal tibia, distal tibia, proximal fibula, proximal metatarsal bone, distal metatarsal bone, proximal phalanx, and/or distal phalanx; in pig no 1 both tracers additionally accumulated in the left distal femur (no osteomyelitis), in left site lymph nodes, and in an abscess next to the calcaneus, but the antibiotic sensitivity indicated that *S. aureus* from the abscess belonged to another strain, different from the inoculated; 2: one additional OM lesion found by histology; 3: two OM lesions found by histology; 4: reisolation of *S. aureus* from OM and/or periosseous abscesses; 5: n.t. not tested; 6: OM positive by microbiology and immunohistochemistry for *S. aureus*; 7: seroma identified; 8: Another strain i.e. MRSA; 9: atelectasis and edema; 10: bronchopneumonia; 11: atelectasis; 12: Not the inoculated S. aureus strain and not MRSA.

There was a moderate and positive correlation between the volume of OM measured on diagnostic CT scans and [^{18}F]FDG uptake indicated by SUV_{max} on day 7 (r=0.45, P=0.033). The [^{99m}Tc]IL8 uptake in OM in the right hind limbs correlated weakly and positively with the volume of OM on CT, however not significantly (r=0.39, P=0.067). There was no difference of [^{99m}Tc]IL8 uptake in OM with neither fistulas compared to OM without fistulas (P=0.135), nor to [^{99m}Tc]IL8 uptake in OM with sequesters versus OM without sequesters (P=0.560). For [^{18}F]FDG uptake with formations of sequesters and fistulous tracts compared to OM lesions without such formations no differences could be detected (P=0.253 for sequester and P=0.093 for fistulous tract formation).

Serum IL8 and CRP

There was a moderate and positive correlation between the volume of the OMs measured on diagnostic CT scans and CRP at day 6 (r=0.5, P=0.037).

[^{99m}Tc]IL8 uptake in the OM lesions as quantitated at day 7 after the inoculation correlated positively with serum IL8 at day 0 (P=0.003), CRP at day 6 (P=0.004), and with [^{18}F]FDG-accumulation in the OM (P=0.017). Neither CRP nor IL8 levels measured in serum correlated at any time points with the [^{18}F]FDG uptake in the OM lesions at day 7 (day 1, 6 and 7; P=0.11, P=0.412, and P=0.88, and P=0.84, P=0.27, and P=0.28).

Discussion

This study showed, that [^{99m}Tc]IL8 is suitable for visualizing OM lesions in peripheral bones of pigs as early as 2 hours after injection of the tracer. Even though there was a diffuse physiological accumulation in the epiphyses/metaphyses of the long bones in pigs, it was possible to differentiate between normal diffuse physiological uptake of [^{99m}Tc]IL8 in bone ends and the increased focal and pathological accumulation in OM lesions in the same locations. A key

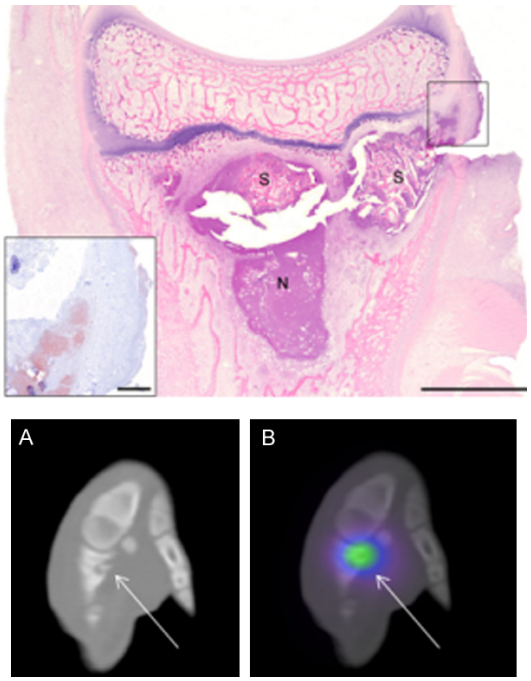

Figure 2. Histopathology, mid-sagittal section of right proximal phalanx from toe IV, pig 9. Osteomyelitis is seen in the metaphysis distal to the growth plate and penetration of the cortical bone by the infection. Sequesters (S) and neutrophils (N) forming an intramedullary abscess close to the growth plate. Bar 4.5 mm. Hematoxylin and Eosin. Insert, immunohistochemically stain for IL8 corresponding to the framed area, and showing large areas of positive cells, primarily neutrophils. Bar 0.54 mm. Below is seen a CT scan (A) and a fusion image of IL8 scintigraphy and CT (B) of the same lesion indicated by arrows.

mechanism of bone marrow stromal cell mediated healing and tissue regeneration is the paracrine secretion of various growth factors and cytokines [47]. Epidermal Growth Factor (EGF) stimulates the gene expression of growth factors and cytokines such as IL8 as well as EGF-receptor ligands [48, 49].

Radiolabeled autologous white blood cells (WBCs) are the gold standard for imaging of various infectious diseases, including OM particularly the appendicular skeleton. Radioactive labelling of autologous leukocytes has some disadvantageous production conditions, and it has been documented that approximately 14% of acute OM lesions may appear as cold lesions on scintigraphy [50], most likely because subperiosteal and intraosseous inflammatory discharge compresses the microcirculation of the involved bone. This compression is thought to occur mainly in the femoral diaphysis and femoral head [16, 51, 52].

We, therefore examined a molecular rather than cellular tracer, namely the [^{99m}Tc]IL8 tracer for detecting OM in a pig model and compared it with [^{18}F]FDG PET as we have had 100% success by demonstrating OM in this model with [^{18}F]FDG [15, 46, 53, 54].

[^{99m}Tc]IL8 offers several advantages compared to radiolabeled leucocytes. The radionuclide [^{99m}Tc] is preferred due to ideal physical characteristics such as short half-life (6 h), ideal energy (140 keV) for scintigraphy, and low radiation burden for the patient, its cost-effectiveness, and the general availability. Preparation of [^{99m}Tc]IL8 is straight forward and rapid with a preparation time of less than 45 minutes and without need for further purification, whereas the preparation of labelled leukocytes is more time-consuming and the living cells should be handled carefully to preserve their viability and their migration capacity. In addition, the need to handle blood with potentially viable microorganisms may pose a risk of transmission to both technicians and patients and should be avoided if possible.

[^{99m}Tc]IL8 accumulated mainly in the kidneys (**Figure 3**). This may be consistent with earlier findings in humans kidneys [40], which do express IL8 [55].

Circulating neutrophils pass through the narrow pulmonary capillary bed. Under normal physiological conditions, there may be longer pulmonary microvascular transit of neutrophils compared to erythrocyte transit in humans [14]. In pigs, the lungs have much of the function of the human spleen, functioning almost like an infection filter [56]. At ~ 230 min after [^{99m}Tc]IL8 injection, this seemed not to be a major interpretation problem, although increased uptake was seen in atelectasis and edematous changes (**Figure 4**). This may indicate that the intravascular macrophages or neutrophils in porcine lungs may possess upregulated IL8 receptors and that the cells may accumulate in congestive/hypostatic atelectasis seen on CT and at necropsy. Another explanation could be that the density of IL8 receptors increases when atelectasis occurs. The infectious foci in the lungs were, however, distinguishable from physiological activity, and [^{99m}Tc]IL8 may be a fair

Table 4. Bio-distribution of [^{99m}Tc]IL8 and [^{18}F]FDG in the pigs without OM and systemic infections

Tracer	Lung	Liver	Spleen	Kidney	Urine	Heart	Brain	Thymus	Small Intestine	Lumbar Vertebra
[^{99m}Tc]IL8 counts/min	450 (196-1021)	695 (433-968)	882 (468-1785)	13578 (1461-32609)	2907 (467-8486)	329 (127-666)	135 (28-505)	210 (123-279)	666 (170-533)	359 (294-1070)
[^{18}F]FDG SUV_{max}	0.6 (0.2-1.0)	1.5 (1.1-1.2)	2.7 (0.5-3.5)	2.4 (1.6-3.5)	53.5 (5.8-84.2)	12 (5.1-22.3)	2.9 (1.8-3.6)	2.4 (1.3-3.1)	2.9 (2.6-4.3)	1.6 (1.3-2.0)

Mean uptake of [^{99m}Tc]IL-8 and [^{18}F]FDG in various organs of the two juvenile pigs without OM.

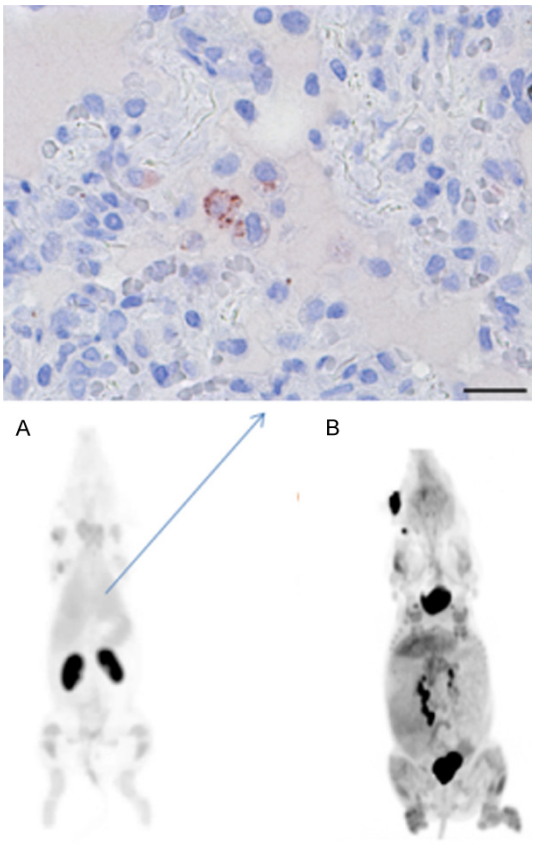

Figure 3. MIPs are showing the biodistribution of [^{99m}Tc]IL8 (A) and [^{18}F]FDG (B) in pig 8 without OM. Above these is shown the immunohistochemically stain for IL8 in the lung (scalebar: 25 µm). There was detectable IL8 in the lung parenchyma in and close to macrophags.

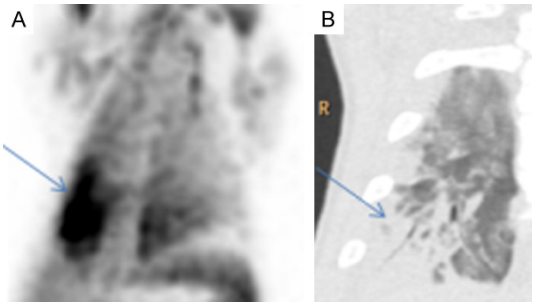

Figure 4. The figure shows [^{99m}Tc]IL8 uptake in pig 2 without OM (A) in atelectasis and edematous changes in the right caudal lung without pneumonia and (B) CT of the same lung. Immunohistochemically stain for IL8 showed no detectable IL8 in the lung parenchyma (not shown). R: Right site.

tracer for infection/inflammation in the lungs of humans when plain radiography and CT cannot provide sufficient information, as IL8 is the

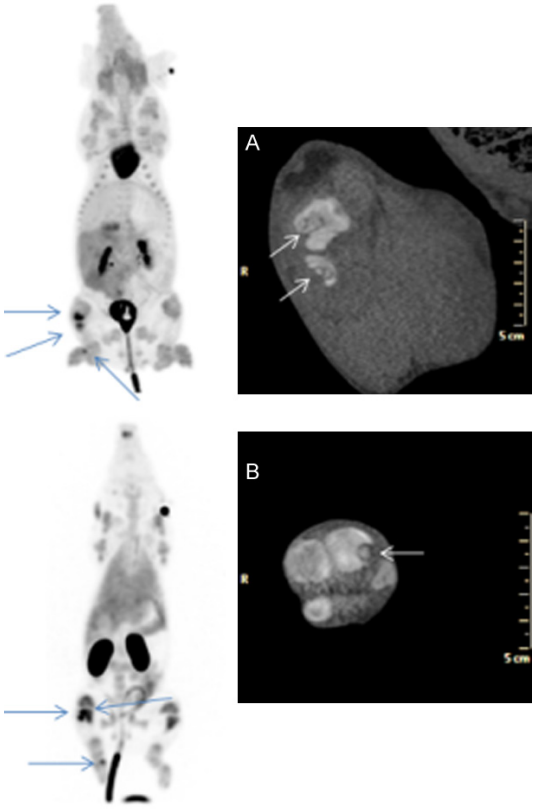

Figure 5. Left: [^{18}F]FDG (maximal intensity projection (MIP), upper) and [^{99m}Tc]IL8 (MIP lower) uptake in pig 4 with 3 osteomyelitis lesions in the right hind limb as indicated by arrows. Right: CT (bone window) of A: osteomyelitis in proximal tibia and fibula, and of B: osteomyelitis in the third metatarsal bone. All OM having formed sequesters and fistulous tracts.The lesions are marked with an arrow. To the right in the CTs is shown a size bar (5 cm).

major neutrophil chemotactic factor in humans [57]. In abscesses, at the site of inoculation, the [^{99m}Tc]IL8 tracer performed well. Normally, early or acute OM is considered to occur within 7 days after inoculation/induction of the infection, but sequester and fistulous tract formation indicates a more advanced stage of the infection [16-18]. Histology also showed a subacute stage of infection. By IHC there were IL8-producing neutrophils and a higher degree of exudation in the periphery of OM. In the center of OM, sequesters occupy the space, which prevent accumulation of neutrophils. Also, IHC often "favours" the peripheral part of a tissue section, which displays the "brightest" IHC staining, probably due to more favorable "concentration gradients" of antibodies along the periphery of the droplets applied to the tissue section. For [^{18}F]FDG, the uptake did not corre-

Table 5. Size of and tracer uptake in osteomyelytis lesions

Size of lesion and tracer uptake	Mean	Minimum	Maximum	SD	Median
OM volume[1] cm^3	0.636	0.01	3.84	0.855	0.360
[^{99m}Tc]IL8 in OM, right limb[2] counts/second	1001	366	2714	552	886
[^{99m}Tc]IL8 in corresponding site without OM, left limb counts/second	439	62	941	283	435
SUV_{max} of [^{18}F]FDG in OM[1] g/mL	4.7	1.0	10.1	2.0	4.5

1: 23 OM lesions; 2: 16 OM lesions. Volumes in cm^3 and uptake of [^{99m}Tc]IL8 in counts per sec and FDG as SUV_{max} in g/mL of 23 osteomyelitis (OM) lesions (of these 16 had IL8-uptake vs. 23 had FDG-uptake). For comparison the uptake of [^{99m}Tc]IL8 in the corresponding anatomical site of the hind limb without OM is shown.

late significantly with the formations of sequesters and fistulous tracts (23 OM lesions). We have, however, previously in a larger experiment (56 OM lesions) found a statistically significant accumulation of [^{18}F]FDG in such formations [56]. In the present study, the same tendencies were seen and the lack of statistical significance may be ascribed to a number-effect as almost all OM had formed sequesters and/or fistulas in the present study, indicating more advanced stages according to Cierny-Mader staging [16-18].

IL8 shows a wide receptor-binding activity across species, including human to pig reactivity [58]; also, porcine and human IL8 amino acid sequences are 73% identical supporting that they will be able to bind to the same receptor [58] and importantly for the study, the affinity of human IL8 for the porcine IL8 receptor (and the homology between the human and the porcine IL8 receptor) resulted in fair imaging of OM in pigs. Human IL8 binding may activate porcine cells which may not be a problem for the labelling itself, however, could be a theoretical problem for the pig resulting in exacerbation of inflammation. We expect that the tracer will perform even better and be more specific in humans.

CRP is a non-specific marker of infection as it increases during inflammation and in cancers, thus reflecting a lot of concomitant processes. To some extent one can argue likewise for neutrophils and other infection/inflammation markers, like e.g. IL8. CRP will be affected by lesions at other locations besides the bones, but the extent of extra-osseous lesions may correlate themselves to the size of lesions in bones. The results from correlating blood infection/inflammation markers to e.g. tracer accumulation should thus be taken with caution and will require a larger sample size. Also, it has earlier been demonstrated that laboratory findings typically show an increase of CRP and erythrocyte sedimentation rate (ESR) especially in acute osteomyelitis in children whilst the white blood count may be normal [4, 59]. We did not measure ESR or daily changes. Our juvenile pigs presented subacute to even chronic OM after just one week.

In conclusion, this study showed that the radiolabelled pro-inflammatory chemotactic chemokine [^{99m}Tc]IL8 visualized OM lesions 7 days after inoculation presumably by targeting the surface receptors on the infiltrating neutrophils. Furthermore, [^{99m}Tc]IL8 performed well detecting 70% of the OM lesions, corresponding to the 78-79% we previously found for [^{111}In]-labelled autologous leucocytes [15, 59]. Our tracer was based on human IL8, and we therefor anticipate the results in humans to be better than in pigs. The quick and simple preparation, early and good image quality, and lower radiation burden suggest that [^{99m}Tc]IL8 may be a suitable imaging alternative for the scintigraphy evaluation of acute OM in children, although less sensitive than [^{18}F]FDG PET.

Acknowledgements

Veterinarian nurse Stine Methmann, Aarhus and animal technician Helle Egeskov Vigen, and as well as the staff at Biomedicinsk Forskningslaboratorium (Dyrestalden) at Aalborg University Hospital are thanked for taking care of the animals. Technicians Janne Frederiksen and Rikke Skall are thanked for planning and performing the scintigraphies. This work was supported by grant no. 0602-01911B (11-107077) from the Danish Council for Independent Research, Technology and Production Sciences.

Disclosure of conflict of interest

None.

Address correspondence to: Pia Afzelius, Department of Nuclear Medicine, Aalborg University Hospital and Nordsjællands Hospital, Dyrehavevej 29, 3450 Hillerød, Aalborg, Denmark. E-mail: pia.afzelius@dadlnet.dk

References

[1] Nickerson EK, Hongsuwan M, Limmathurotsakul D, Wuthiekanun V, Shah KR, Srisomang P, Mahavanakul W, Wacharaprechasgul T, Fowler VG, West TE, Teerawatanasuk N, Becher H, White NJ, Chierakul W, Day NP and Peacock SJ. Staphylococcus aureus bacteremia in a tropical setting: patient outcome and impact of antibiotic resistance. PLoS One 2009; 4: e4308.

[2] Pääkkönen M, Kallio PE, Kallio MJ and Peltola H. Management of osteoarticular infections caused by staphylococcus aureus is similar to that of other etiologies. Pediatr Infect Dis J 2012; 31: 436-438.

[3] Riise ØR, Kirkhus E, Handeland KS, Flatø B, Reiseter T, Cvancarova M, Nakstad B and Wathne KO. Childhood osteomyelitis-incidence and differentiation from other acute onset musculoskeletal features in a population-based study. BMC Pediatr 2008; 8: 45-54.

[4] Hatzenbuehler J and Pulling TJ. Diagnosis and management of osteomyelitis. Am Fam Physician 2011; 84: 1027-1033.

[5] Johansen LK and Jensen HE. Animal models of hematogenous staphylococcus aureus osteomyelitis in long bones: a review. Orthop Res Rev 2013; 5: 51-64.

[6] Alstrup AK, Nielsen KM, Schønheyder HC, Jensen SB, Afzelius P, Leifsson PS and Nielsen OL. Refinement of a hematogenous localized osteomyelitis model in pigs. Scand J Lab Anim Sci 2016; 42: 1-4.

[7] Jaramillo D. Infection: musculoskeletal. Pediatr Radiol 2011; 41: S127-134.

[8] Pineda C, Espinosa R and Pena A. Radiographic imaging in osteomyelitis: the role of plain radiography, computed tomography, ultrasonography, magnetic resonance imaging and scintigraphy. Semin Plast Surg 2009; 23: 80-89.

[9] Godoy IRB, Neto LP, Rodrigues TC and Skaf A. Intra and extramedullary fat globules as an MRI marker for osteomyelitis. Radiol Case Rep 2018; 13: 1228-1232.

[10] Mettler F and Guiberteau M. Chapter 8: skeletal system. In: Mettler F, Guiberteau M, editors. Essentials of Nuclear Medicine Imaging. 6th edition. Philadelphia, PA: Saunders Elsevier; 2012. pp. 296-300.

[11] Santiago Restrepo C, Gimenez CR and McCarthy K. Imaging of osteomyelitis and musculoskeletal soft tissue infections: current concepts. Rheum Dis Clin North Am 2003; 29: 89-109.

[12] Littenberg B and Mushlin AI. Technetium bone scanning in the diagnosis of osteomyelitis: a meta-analysis of test performance. Diagnostic technology assessment consortium. J Gen Intern Med 1992; 7: 158-164.

[13] Van den Wyngaert T, Strobel K, Kampen WU, Kuwert T, van der Bruggen W, Mohan HK, Gnanasegaran G, Delgado-Bolton R, Weber WA, Beheshti M, Langsteger W, Giammarile F, Mottaghy FM and Paycha F; EANM Bone & Joint Committee and Oncology Committee. The EANM practice and guidelines for bone scintigraphy. Eur J Nucl Med Mol Imaging 2016; 43: 1723-1738.

[14] Parisi MT, Otjen JP, Stanescu AL and Shulkin BL. Radionuclide imaging of infections and inflammation in children: a review. Semin Nucl Med 2018; 48: 148-165.

[15] Afzelius P, Alstrup AK, Schønheyder HC, Borghammer P, Jensen SB, Bender D and Nielsen OL. Utility of ^{11}C-methionine and ^{11}C-donepezil for imaging of *Staphylococcus aureus* induced osteomyelitis in a juvenile porcine model: comparison to autologous ^{111}In-labelled leukocytes, ^{99m}Tc-DPD, and ^{18}F-FDG. Am J Nucl Med Mol Imaging 2016; 6: 286-300.

[16] Calhoun JH, Manring MM and Shirtliff M. Osteomyelitis of the long bones. Semin Plast Surg 2009; 23: 59-72.

[17] Carek PJ, Dickerson LM and Sack JL. Diagnosis and management of osteomyelitis. Am Fam Physician 2001; 63: 2413-2420.

[18] Lazzarini L, Mader JT and Calhoun JH. Osteomyelitis in long bones. J Bone Joint Surg Am 2004; 86-A: 2305-2318.

[19] Roca M, de Vries EFJ, Jamar F, Israel O and Signore A. Guidelines for the labelling of leucocytes with ^{111}In-oxine. Eur J Nucl Med Mol Imaging 2010; 37: 835-841.

[20] Al-Sheikh W, Sfakianakis GN, Mnaymneh W, Hourani M, Heal A, Duncan RC, Burnett A, Ashkar FS and Serafini AN. Subacute and chronic bone infections: diagnosis using In-111, Ga-67 and Tc-99m MDP bone scintigraphy, and radiography. Radiol 1985; 155: 501-506.

[21] Termaat MF, Raijmakers PG, Scholten HJ, Bakker FC, Patka P and Haarman HJ. The accuracy of diagnostic imaging for the assessment of chronic osteomyelitis: a systematic review and meta-analysis. J Bone Joint Surg Am 2005; 87: 2464-2471.

[22] Luster AD. Chemokines-chemotactic cytokines that mediate inflammation. N Engl J Med 1998; 338: 436-445.

[23] Zurek OW, Pallister KB and Voyich JM. Staphylococcus aureus inhibits neutrophil-derived

IL-8 to promote cell death. J Infect Dis 2015; 212: 934-938.
[24] Zeilhofer HU and Schorr W. Role of interleukin-8 in neutrophil signalling. Curr Opin Hematol 2000; 7: 178-182.
[25] Scapini P, Lapinet-Vera JA, Gasperini S, Calzetti F, Bazzoni F and Cassatella MA. The neutrophil as a cellular source of chemokines. Immunol Rev 2000; 170: 195-203.
[26] Tecchio C, Micheletti A and Cassatella MA. Neutrophil-derived cytokines: facts beyond expression. Front Immunol 2014; 5: 1-7.
[27] Sadik CD, Kim ND and Luster AD. Neutrophils cascading their way to inflammation. Trends Immunol 2011; 32: 452-460.
[28] Harada A, Sekido N, Akahosi T, Wada T, Mukaida N and Mat sushima K. Essential involvement of interleukine-8 (IL-8) in acute inflammation. J Leukoc Biol 1994; 56: 559-564.
[29] Strieter RM, Kasahar K, Allen RM, Standiford TJ, Rolfe MW, Becker FS, Chensue SW and Kunkel SL. Cytokine-induced Neutrophil-derived Interleukin-8. Am J Pathol 1992; 141: 397-407.
[30] Goodman RB, Forström JW, Osborn SG, Chi EY and Martin TR. Identification of two neutrophil chemotactic peptides produced by porcine alveolar macrophages. J Biol Chem 1991; 266: 8455-8463.
[31] McILwain RB, Timpa JG, Kurundkar AR, Holt DW, Kelly DR, Hartman YE, Neel M, Karnatak RK, Schelonda R, Anantharamaiah GM, Killingsworth CR and Maheshwarl A. Plasma concentrations of inflammatory cytokines rise rapidly during ECMO-related SIRS due to the release of preformed stores in the intestine. Lab Invest 2010; 90: 128-139.
[32] van Malenstein H, Wauters J, Mesotten D, Langouche L, De Vos R, Wilmer A and van Pelt J. Molecular analysis of sepsis-induced changes in the liver: microarray study in a porcine model of acute fecal peritonitis with fluid resuscitation. Shock 2010; 34: 427-436.
[33] Rothe L, Collin-Osdoby P, Chen Y, Sunyer T, Chaudhary L, Tsay A, Goldring S, Avioli L and Osdoby P. Human osteoclasts and osteoclast-like cells synthesize and release high basal and inflammatory stimulated levels of the potent chemokine interleukin-8. Endocrinol 1998; 139: 4353-4363.
[34] Bendre MS, Montague DC, Peery T, Akel NS, Gaddy D and Suva LJ. Interleukin-8 stimulation of osteoclastogenesis and bone resorption is a mechanism for the increased osteolysis of metastatic bone disease. Bone 2003; 33: 28-37.
[35] Kopesky P, Tiedemann K, Alkekhia D, Zechner C, Millard B, Schoeberl B and Komarova SV. Autocrine signaling is a key regulatory element during osteoclastogenesis. Biol Open 2014; 3: 767-776.
[36] Gross MD, Shapiro B, Fig LM, Steventon R, Skinner RW and Hay RV. Imaging of human infection with (131)I-labeled recombinant human interleukin-8. J Nucl Med 2001; 42: 1656-1659.
[37] Rennen H, Boerman OC, Oyen W and Corstens F. Labeling method largely affects the imaging potential of interleukin-8 [letter]. J Nucl Med 2002; 43: 1128.
[38] Heegaard PMH, Pedersen HG, Jensen AL and Boas U. A robust quantitative solid phase immunoassay for the acute phase protein C-reactive protein (CRP) based on cytidine 5'-diphosphocholine coupled dendrimers. J Immunol Meth 2009; 343: 112-118.
[39] Aalbæk B, Jensen LK, Jensen HE, Olsen JE and Christensen H. Whole-genome sequence of *Staphylococcus aureus* S54F9 isolated from a chronic disseminated porcine lung abscess and used in human infection models. Genome Announc 2015; 3.
[40] Bleeker-Rovers CP, Rennen HJ, Boermann OC, Wymenga AB, Visser EP, Bakker JH, van der Meer JW, Corsten FH and Oyen WJ. 99m Tc-labbeled interleukin 8 for scintigraphic detection of infection and inflammation: first clinical evaluation. J Nucl Med 2007; 48: 337-343.
[41] Jødal L, Afzelius P and Jensen SB. Influence of positron emitters on standard gamma-camera imaging. J Nucl Med Tech 2014; 42: 42-50.
[42] Madsen LW and Jensen HE. In: Jensen HE, editor. Necropsy of the Pig. Necropsy a handbook and atlas. Frederiksberg: Biofolia; 2011. pp. 83-106.
[43] Jensen HE, Nielsen OL, Agerholm JS, Iburg T, Johansen LK, Johannesson E, Møller M, Jahn L, Munk L, Aalbæk B and Leifsson PS. A non-traumatic staphylococcus aureus osteomyelitis model in pigs. In Vivo 2010; 24: 257-264.
[44] Christiansen JKG, Jensen HE, Johansen LK, Koch J, Aalbæk B, Nielsen OL and Leifsson PS. Systemic inflammatory response and local cytokine expression in porcine models of endocarditis. Acta Pathol Microbiol Immunol Scand 2014; 122: 292-300.
[45] Chung M. Correlation coefficient. In: Salkin NJ, editor. Encyclopedia of measurement and statistics. London: Sage Publications; 2007. pp. 189-201.
[46] Afzelius P, Nielsen OL, Alstrup AKO, Bender D, Leifsson PS, Jensen SB and Schønheyder HC. Biodistribution of the radionuclides ^{18}F-FDG, 11C-methionine, 11C-PK11195, and 68Ga-citrate in domestic juvenile female pigs and morphological and molecular imaging of the tracers in hematogenously disseminated staphylococcus aureus lesions. Am J Nucl Med Mol Imaging 2016; 6: 42-58.

[47] Wagner EF. Bone development and inflammatory disease is regulated by AP-1 (Fos/Jun). Ann Rheum Dis 2010; 69: i86-88.
[48] Eccles SA. The epidermal growth factor receptor/Erb-B/HER family in normal and malignant breast biology. Int J Dev Biol 2011; 55: 685-696.
[49] Müller-Deubert S, Seefried L, Krug M, Jakob F and Ebert R. Epidermal growth factor as a mechanosensitizer in human bone marrow stromal cells. Stem Cell Res 2017; 24: 69-76.
[50] Datz LF and Thorne DA. Cause and significance of cold bone defects on indium-111-labeled leukocyte imaging. J Nucl Med 1987; 28: 820-823.
[51] Kumar V, Abbas AK, Fausto N and Mitchell RN. Robbins basic pathology. 8th edition. Saunders Elsevier; 2007. pp. 810811.
[52] Emslie KR, Ozanne NR and Nade SM. Acute haematogenous osteomyelitis: an experimental model. J Pathol 1983; 141: 157-167.
[53] Afzelius P, Nielsen OL, Schønheyder HC, Alstrup AK and Hansen SB. An untrapped potential for imaging of peripheral osteomyelitis in paediatrics using [^{18}F]FDG PET/CT -the inference from a juvenile porcine model. EJNMMI Res 2019; 9: 29-37.
[54] Afzelius P, Nielsen OL, Jensen SB and Alstrup AK. Post mortem leukocyte scintigraphy in juvenile pigs with experimentally induced osteomyelitis. Contrast Media Mol Imaging 2017; 2017: 3603929.
[55] Niemir ZI, Stein H, Ciechanowicz A, Olejniczak P, Dworacki G, Ritz E, Waldherr R and Czekalski S. The in situ expression of interleukin-8 in the normal human kidney and in different morphological forms of glomerulonephritis. Am J Kidney Dis 2004; 43: 983-998.
[56] Ricci MA, Mehran R, Christou NV, Mohamed F, Graham AM and Symes JF. Species differences in the clearance of Staphylococcus aureus bacteremia. J Invest Surg 1991; 4: 53-58.
[57] Kunkel SL, Standiford T, Kasahara K and Strieter RM. Interleukin-8 (IL-8): the major neutrophil chemotactic factor in the lung. Exp Lung Res 1991; 17: 17-23.
[58] Scheerlinck JP. Functional and structural comparison of cytokines in different species. Vet Immunol Immunopathol 1999; 72: 39-44.
[59] Dartnell J, Ramachandran M and Katchburian M. Haematogenous acute and subacute paediatric osteomyelitis. J Bone Joint Surg 2012; 94: 584-595.